Preprint

Economics of Induction Linac Drivers for Radiation Sources

William A. Barletta

June 15, 1987

For submission to:
Adriatico Conference on
Undulator Magnets for Synchrotron
Radiation and Free Electron Lasers,
International Center of Theoretical Physics
Trieste, Italy, 23-26 June 1987

Beam Research Program

Disclaimer

Economics of Induction Linac Drivers for Radiation Sources*

William A. Barletta

Lawrence Livermore National Laboratory
University of California, Livermore, California 94550

Abstract

Recent developments in high reliability components for linear induction accelerators (LIA) make possible the use of LIAs as large-scale, economical sources of radio-frequency (rf) power for many applications. One particularly attractive example of interest to high energy physicists is a "two-beam accelerator" version of a linear e^+- e^- collider at TeV energies in which the LIA is configured as a monolithic relativistic klystron operating at 10 to 12 GHz. Another example of keen interest to the fusion community is the use of the LIA to drive a free-electron laser operating at 200 to 500 GHz for use in heating fusion plasmas via electron resonance cylotron heating. This paper briefly describes several potential uses of LIA radiation sources. It discusses the physical basis for scaling our present experience with LIAs to the operating characteristics applicable to large-scale sources of rf power and synchroton radiation.

1. Motivation

1.1 Directly Driven Radiation Sources

1.1.1 Linear Colliders.

The desire of high energy physicists to investigate phenomena at TeV energies has lead accelerator designers to consider new classes of machines that can

* Work performed jointly under the auspices of the U.S. Department of Energy by the Lawrence Livermore National Laboratory under contract No. W-7405-Eng-48 and by the Lawrence Berkeley Laboratory for the Office of Energy Research of the U.S. Department of Energy under contract DE-AC03-76SF00098.

achieve accelerating gradients >100 MeV/m in structures suitable for high repetition rate operation. The approach should be highly reliable and highly energy efficient if the costs of machine operation are to remain within currently acceptable bounds. In general, the accelerating gradient can be increased and the energy required per meter of accelerator structure reduced by scaling[1] the (effective) rf-structure of the accelerator to high frequencies (≥10 GHz.) The practical limits of this approach for conventional rf-cavities are set by the electron-induced breakdown limit and the surface heating limit, with little gain in gradient being achievable for frequencies exceeding 30 GHz. Considering that the cost of the rf-structure is likely to increase once it is miniaturized beyond a scale size of about 2 cm, we can select 10 to 30 GHz as the best frequency range for an advanced linear collider.

At the low end of this frequency range we can employ many conventional klystrons to power the collider. More novel approaches, however, may offer the same performance at substantially lower cost. The two-beam accelerator (TBA) is a concept for using the high peak current beam produced with an linear induction accelerator (LIA) to excite an rf-generating structure at high frequency; the high peak power rf is then fed via a transfer structure to the miniaturized rf-cavities of the high gradient (200 - 400 MeV/m) accelerator of the high energy beam. One variant of the TBA[2] employs a free-electron laser amplifier to transform the kinetic energy of the high current beam to high peak power microwaves. Figure 1 illustrates another variant[3], more suitable to the frequency range from 10 to 15 GHz; this approach converts the LIA into a monolithic relativistic klystron that runs the length of the high frequency rf-accelerator. Although both of these concepts are at relatively early stages of evaluation, the full-scale systems for both approaches involve driving beams already available with state-of-the art induction linacs at Lawrence Livermore National Laboratory (LLNL).

1.1.2 Heating Fusion Plasmas

Our recent success[4] at converting the kinetic energy of a high current electron beam into microwave energy with an efficiency of ≈40% has sparked considerable interest in the magnetic fusion community in the US, Japan, and Italy in using LIAs operating at multi-kHz repetition rates to provide megawatts of time-average submillimeter wave power to heat plasmas in high field tokamaks via electron cylotron resonance heating (ERCH). Moreover, the high peak powers available seem to hold the promise of providing dc-current drive for tokamaks. The use of the FEL as a high power microwave amplifier seems to hold a further advantage of allowing tuning of the frequency of the microwave power over a 10% frequency range during a 1- to 10-millisecond period. This concept will be

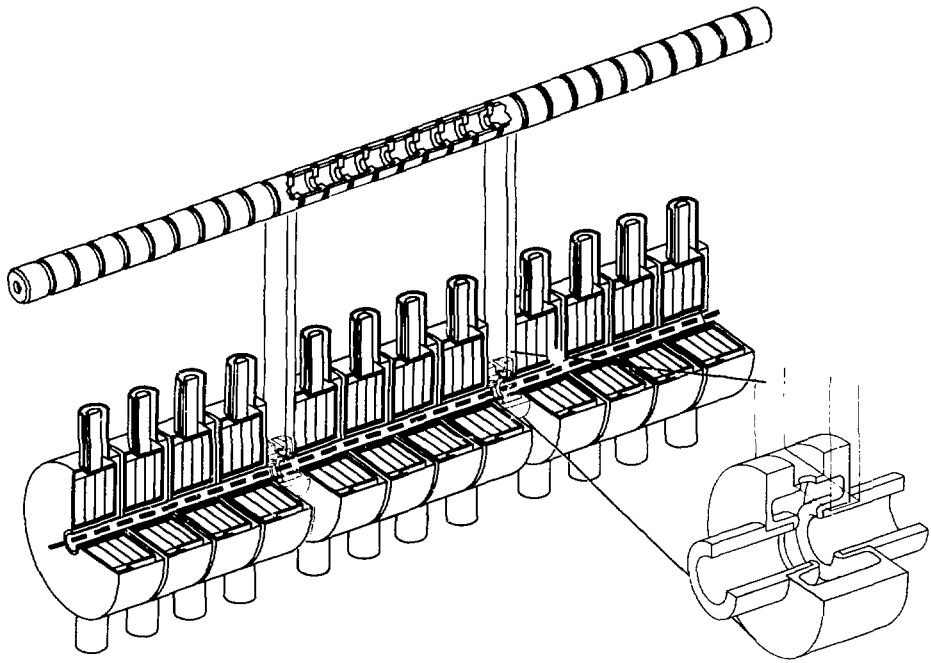

Figure 1. Schematic of a relativistic klystron.

explored[5] experimentally at LLNL in the MTX experiment in which the Alcator C tokamak will be driven by ≈2 MW of microwaves at 250 to 400 GHz.

Induction linacs for this application will typically be sized to provide a 1- to 3-kA, 40- to 100-ns, pulsed electron beam at 8 to 10 Mev. Operating the linac at a repetition rate of 3 to 5 kHz should provide 1 to 3 MW of rf power. For the 10 to 20 MW of rf power generally considered necessary to heat an ignition scale fusion device, multiple linacs supplying ≈2 MW increments of power appear to provide the most practical approach.

1.2. Indirect Drivers

1.2.1 Compact UV Sources

The relativistic klystron illustrated in Fig. 1 can be scaled to the ≈0.5- to 2-GeV energy range to be combined with a very high brightness photo-cathode electron

gun. Extracting a peak current from the gun of 500 to 1000 A would allow the operation of a high gain FEL amplifier in the spectral range of 100 to 500 nm. Although the ultra-high gradient rf linac is not essential for such an FEL, its use may make this approach to generating tunable UV radiation available to far more institutions than could afford and house a conventional high energy electron accelerator. The induction drivers for such lasers would accelerate 1 to 2 kA of 40- to 70-ns electron beam pulses to ≈7 MeV. Deceleration of the drive beam by klystron cavities would provide enough microwave power for a ≈1-GeV compact accelerator.

The idea of minaturizing synchrotron sources by using high gradient rf-structures can be extended to include storage rings. Provided that superconducting magnets with sufficient field strengths can be fabricated, the LIA-driven rf-sources needed for linear colliders can provide sufficient power to compensate for the increased energy losses in a compact ring. Of course, the GeV-class injector to the storage ring can be a high gradient linac driven by a relativisitic klystron.

1.2.2 Hard Gamma Sources

An unusual incoherent source[6] of 50- to 1000-MeV gammas can be provided from a compact 10-GeV linac equipped with the "beamsstrahlung converter" illustrated in Fig. 2. The converter is a region of megagauss fields in which the beam rapidly decelerates by emitting incoherent synchrotron radiation. The large magnetic field need not be applied externally; it can be generated by the beam itself. This process, magnetic bremsstrahlung ("beamsstrahlung"), has the added advantage of radically transforming the energy distribution of the emitted radiation to one peaked at very high energy (>>10 MeV).

For a 10-GeV beam with a peak current of 500 A and with a self-focused beam radius of 1 μm the confining pinch field of such a beam will be 1 MG. The electrons in the confined beam will undergo betatron motion with a mean angle and wavelength

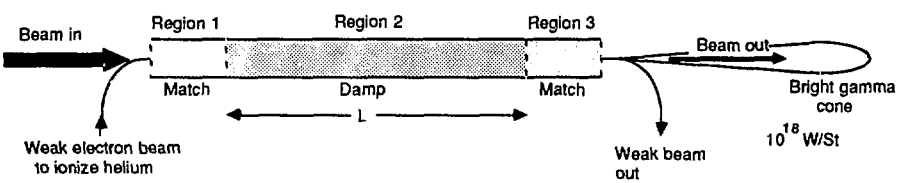

Figure 2. Schematic of incoherent synchrotron source with megagauss fields.

$$\theta_\beta = 1.2 \times 10^{-3} \text{ rad} ,$$
$$\lambda_\beta = 0.52 \text{ cm} . \quad (1)$$

The temporal frequency of the electron oscillations is

$$\Omega = c / \lambda_\beta = 5.7 \times 10^{10} \text{ Hz} . \quad (2)$$

Electrons experiencing such rapid oscillations will emit copious synchrotron radiation, thereby losing energy and shrinking in radius with an e-folding length[7],

$$L_B = 8 \times 10^3 (a / 8.7 \ \mu\text{m})^2 (2 \times 10^4 / \gamma) (250 \text{ A} / I_{eff})^2 \text{ meters} ,$$
$$= 28 \text{ m} . \quad (3)$$

The angular width of the synchrotron radiation is somewhat narrower than (approximately half) the betatron angle, which will expand by $\sqrt{e}$ in the process. For the electron beam to create the strong pinch field, the beam's space charge must be neutralized. The neutralization can be accomplished by injecting the beam into a tube of length, L_B, filled with low pressure gas with a large radiation length. Helium at ≈20 Torr will provide sufficient background ions to focus the beam, while constituting only 6×10^{-4} radiation lengths of scatterer. The multiple scattering in the beamsstrahlung converter leads to a scattering angle of 15 μrad, a value much smaller than the betatron angle.

The most startling feature of the beamsstrahlung converter is the hardness of the radiation that possesses a synchrotron spectrum, characterized by a critical frequency above which few gammas are generated. The critical frequency, ω_c, is given by

$$\omega_c = 3 (\omega_0 \gamma^3) , \quad (4)$$

where ω_0 is the frequency of the electrons' motion in the laboratory frame. For example, the betatron wavelength is 0.5 cm, corresponding to a frequency of 6×10^{10} Hz. From Eq. (4) we obtain a critical frequency of 1.4×10^{24} Hz. Recalling that 1 eV = 2×10^{14} Hz, we find that the critical energy is ≈7 GeV. Although this value is nearly equal to the incident beam energy, the quantum mechanical correction to the classical synchrotron distribution is not substantial since nearly all frequencies are kinematically allowed. The peak of the frequency distribution is at ≈1.5 GeV with substantial radiation down to 50 MeV.

The induction linac suitable for driving this incoherent source would be a ≈50-MeV, 3-kA, 50-ns machine. Such an accelerator could operate at repetition rates up to 5000 kHz. With this driver the gamma source would have a peak brightness of 10^{18} W/St and an average brightness as high as 10^{14} W/St.

2. Principles of Induction Linac Design

Reference 8 presents detailed scaling relations suitable to estimate LIA costs over the wide range of operating parameters appropriate to the several varieties of radiation sources described above. Scaling relations from Ref. 8 are reprinted in the Appendix. This section discusses the principles of LIA design consistent with the constraints of beam dynamics and properties of materials from which the scaling relations are derived. The scaling variables for the LIA include beam voltage, V, beam current, I, pulse length, T_p, repetition rate, f, and gradient, G, in the induction modules.

The injector and accelerator cells consist of nonresonant, axisymmetric gap structures that enclose toroidal cores of ferromagnetic material such as ferrite. A drive voltage impressed across the gap by the power drive changes the flux in the core, inducing an axial electric field that accelerates the electrons. In general, the electron injector and accelerator cells have similar power drive networks (Fig. 3): a dc-power supply charges a set of intermediate storage capacitors via a command resonant charging circuit. These intermediate stores are discharged through the primary commutators--thyratrons (or SCRs)--into low impedence

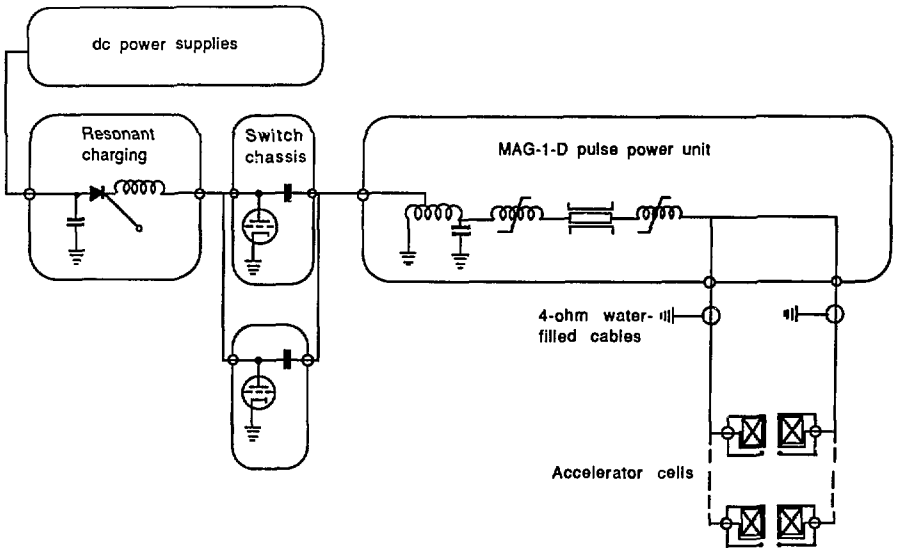

Figure 3. Schematic of baseline design of induction linac.

magnetic pulse compressors (MAG)[9]. Each compressor powers a number of accelerator cells connected in parallel. Although the high current beam (≥1 kA) provides the primary load for the pulse compressors, a parallel compensation network maintains a constant accelerating voltage throughout the beam pulse. The fundamental limits to the operating characteristics of the LIA are set by beam transport physics, material properties, and primary commutator recovery times.[10]

2.1 Injector Scaling

The injector scaling assumes a gridless, constant perveance design with space-charge-limited emission, i.e., the injector voltage, V_{inj}, supplied by muliple induction cells is given by

$$V_{inj} = k\,(I_{beam})^{2/3} \qquad (5)$$

where V_{inj} is in MeV, I_{beam} is in kA, and k = 0.75 (1.45) for high current (brightness) beams. The scaled designs employ a thermionic (dispenser) cathode. The primary cost components include the injector induction structure, focusing, MAG drives, intermediate stores and power supplies, alignment fixtures, and vacuum. Ancillary systems include vacuum and gas handling sytems, low and extremely low conductivity water (LCW), electrical fluids such as insulating fluids and compensation loads, alignment fixtures, miscellaneous fixtures and structures, and instrumentation and controls.

2.2. Accelerator Cell and Drive Design

A suitable basis for scaling the design of the accelerator cells and drives is the prototype of the ETA II cell illustrated in Fig. 4, the MAG-1-D[11] pulse compressor, and its associated thyratron-switched intermediate energy stores. The key cell characteristics are the gap width, w, the inner radius of the cell, r_i, the radius of the beampipe, b, and the volt-seconds of core material. The cores consist of toroids of ferrite (TDK PE-11), which has minimal core losses for short saturation times (<1 μs). The gap size and shape is selected to minimize the Q of the cell and Z , the coupling of the beam to transverse (beam breakup) modes of the cell. The baseline design has a gap width, w, of 0.635 cm for a conservatively chosen gap stress, E_g, of 175 kV/cm. The insulator, which separates the vacuum from the insulating fluid (FC-75), is set at an angle that allows all TM cavity modes to pass through the insulator without reflection to be absorbed by the ferrite. The slight reentrant design of the gap shields the insulator from stray beam electrons. The difference

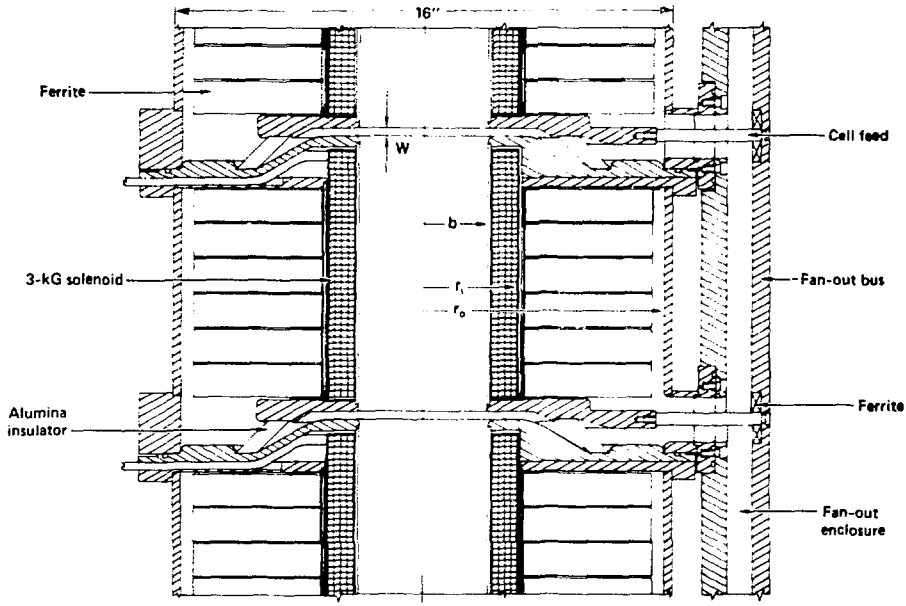

Figure 4. Typical cross-section of low-gamma ten-cell module.

between the pipe size and inner cell radius (≈2 cm) is accounted for by the size of steering magnets, focusing magnets (~1 to 3 kG), and spacers to allow insulating fluid to flow along the inner boundaries of the ferrite.

The choice of inner radius (7.5 cm) for the baseline design was set to keep the beam breakup (BBU) growth below 10 in an accelerator for a mono-energetic, 3-kA beam transported with quadrupoles through ~10^3 gaps (accelerating cavities). With such a focusing system, the beam breakup growth, S, will scale as

$$S \propto I_{beam}\,(w/b^2)\,(\ln N_g)\,\mathrm{Im}\,P_1(\omega)/BE_g \quad , \qquad (6)$$

where N_g is the number of gaps and B is the (effective) field strength of the magnetic transport. Typically, we can replace the beampipe radius, b, in Eq. (6) with r_i for the purpose of scaling costs. The quantity Im $P_1(\omega)$ is that part of the cavity response function that produces growth of TM_{1n0} beam breakup modes. To suppress BBU we minimize |Im $P_1(\omega)$| by arranging that the beam induced fields in the cavity are purely outgoing. That is, we shape the gap so as to approxima'e

a perfectly matched radial line. In that case[12], $|\,\mathrm{Im}\,P_1(\omega)\,|$ is a slowly varying value of w/b and is roughly linear over the range $0.1 < w/b < 1$;

$$|\,\mathrm{Im}\,P_1(\omega)\,| \approx 0.71 - 0.33\, w/b \ . \tag{7}$$

Typically, in induction linacs built to date, b is several centimeters, and w/b is ≈0.3. In contrast, the relativistic klystron variant of the TBA will require a pipe size <1 cm (beyond cutoff) in which case w/b > 1. Two factors suppress the BBU in this case; for the accelerator cells, w/b ≈ 3 at which the value $|\,\mathrm{Im}\,P_1(\omega)\,|$ is on the order of 10^{-2}.

For several of the scenario described above the LIA is converted into a relativistic klystron. In that case we must reassess the transverse stability of the beam. The BBU growth due to the beam interaction with the klystron cavity is rapid. Almost as rapid is the growth of transverse motion due to the resistive wall instability.[13] Fortunately, the large spread in the beam's betatron frequency due to the large energy spread induced by the klystron action and/or by laser-guided transport[14] allows shrinking the pipe size below cutoff (r_i = 2.5 cm) as is required for the operation of the klystron.

The outer radius of the cell is determined by the accelerating voltage, V_{acc}, and the cell length, z, via the magnetic induction equation,

$$V_{acc}\, T_p = A\, (\Delta B) \tag{8}$$

where A is the cross-sectional area of the ferrite, ΔB is the total flux swing (0.6 Wb/m^2), and T_p is the pulse duration. We can recast Eq. (8) in terms of the effective gradient, G, and the packing fraction for the ferrites, p, as

$$r_o = r_i + (G\, T_p / p) / \Delta B \ . \tag{9}$$

Typically, the packing fraction is 0.8. Effective gradients, G, may range from 0.75 to 1.5 MeV/m.

The beam transport system is simplified if the accelerating voltage varies over time by no more than 1%. In that case the length of the cell and the properties of the ferromagnetic material are subject to an additional constraint. The region between the high voltage drive blade and the back wall of the induction cavity should be designed to be a constant impedance transmission line loaded with a high μ material to slow the wave speed. Even if the transverse dimension of the cavity is sufficiently large to avoid a saturation wave forming in the core, the transit time in the longitudinal direction must equal or exceed the pulse length; that is,

$$z \geq Tp\ (\mu\varepsilon)^{1/2} \ . \tag{10}$$

Moreover, for the transmission line have a constant impedance the core must be composed of a material like ferrite rather than wound metallic glass tapes. For high fidelity ferrites

$$(\mu\varepsilon)^{1/2} \approx 100 \ ; \tag{11}$$

hence, Eq. (5) can be written as

$$c(r_o\text{-}r_i) \,/\, (\mu\varepsilon)^{1/2} \geq (V/\Delta B) \ . \tag{12}$$

If the core geometry is such that the value of the magnetic field in the core varies inversely with radius, then to avoid saturation anywhere in the core Eq. (12) should be modified to

$$c(r_o\text{-}r_i) \,/\, (\mu\varepsilon)^{1/2} \geq [\ln (r_o/r_i)]\ (V/\Delta B) \ . \tag{13}$$

For both compactness and convenience in installation and maintenance, the accelerator cells are packaged in blocks of ten. Attaching each block to a strongback structure assures accelerator alignment to better than 0.5 mm. If the beam transport is provided by a laser-ionized channel, or if the energy spread in the beam is large (as in the case of the relativistic klystron configuration), the structural demands on the strongback are eased considerably, because the cell blocks can have a smaller inner radius and therefore can be shorter and lighter.

For high average power applications such as heating plasmas or powering linear colliders the need to minimize operating costs implies keeping core magnetization (hysterisis) losses small. This design consideration also reduces beam energy variations during the pulse ($\Delta E/E < 1\%$). In practical terms, the magnetization current should not exceed 20% of the beam current, i.e.,

$$I_m = (1/L) \int V_{acc}\, dt \ \leq 0.2\ I_{beam} \ , \tag{14}$$

where L, the core inductance, is given by

$$L = (\mu/2\pi)\ z \ln (r_o/r_i) \ . \tag{15}$$

Then, the core loss per pulse (joules per volt) is

$$\Re = (\pi/\mu)\ G\ T_p^2\ (\ln r_o/r_i)^{-1} \ . \tag{16}$$

For the ETA II core, T_p = 75 ns and $\Re$ = 16 J/MV; reducing T_p to 50 ns would reduce $\Re$ to <9 J/MV. For relativistic klystrons designed to power large linear colliders (~4 GV of induction cells per TeV of high energy linac), the incentives to lower T_p are clear.

The power drives are freon-cooled magnetic modulators, MAG-1-Ds, which consist of metallic glass, nonlinear inductors that operate from the unsaturated to fully saturated state in the pulse compression process. For LIAs operating at repetition rates between 100 to 1000 Hz, the MAG-1-D pulse compressors are capable of continuous operation[10] and have been tested for hundreds of millions of pulses without change in operating characteristics. At the upper end of this range the primary commutators must be ceramic-envelope thyratrons capable of high temperature operation. At 100 to 200 Hz glass-envelope tubes will suffice at one third the cost.

2.3. Scaling Principles

By breaking down each subsystem of the accelerator into a set of components and their internal constituents (if necessary) we arrive at a descriptive level at which scaling relations can be assigned on the basis of fundamental physical characteristics. For example, the cost of the accelerator cell housing is determined by the quantity of metal and, more significantly, by the length of machining, finishing and welding time involved in the cell manufacture. This fabrication time scales linearly with the surface area to be machined, finished, welded, and inspected. This scaling procedure does not account for savings through the use of "production engineering techniques", such as large-scale metal casting, robot welding, etc. Such techniques could reduce the cost of the accelerator cell housings by more than 30%. Table 1 presents the physical principles upon which scaling of the accelerator components are based. Quantitative scaling relations from Ref. 8 are reprinted in the Appendix.

3. Conclusions

The design considerations described above enable us to estimate the costs of LIA-driven radiation sources over the wide range of operating specifications relevant to the applications described in Sec. 1. For example, making compact rf-linacs requires generating stronger rf-fields at higher frequencies than present tubes can supply. These higher fields imply much higher peak powers than present klystrons deliver. Consequently, the costs of compact rf-accelerators may be prohibitive unless LIA-driven sources can provide power at significantly lower

Component	Internals	Scaling
Power supplies	DC supplies CRCs	Average power
Intermediate stores	Capacitors Thyratrons	Pulse energy Average current, pulse energy
Magnetic compressors	MAG-1-D	Pulse energy
Accelerator cells	Ferrites Cell housing, gap	Volume (V_{acc}, T, G) Surface area (r_i, r_o, G) Total voltage
Strongback		Cell weight & length

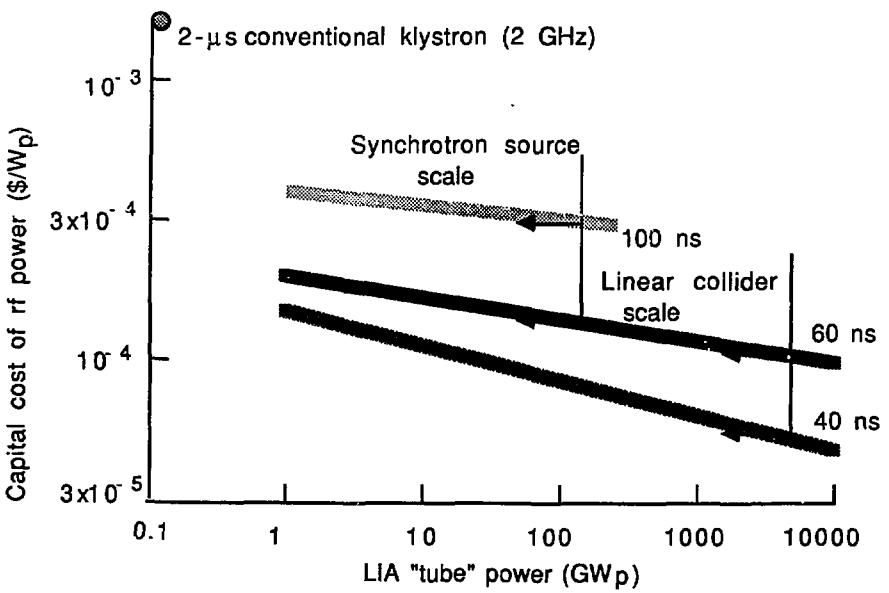

Figure 5. Cost of LIA-generated microwave power.

cost than klystrons. Figure 5 illustrates how the cost of rf power delivered by a LIA-driven relativistic klystron drops with as the size of the power source increases. It compares these estimates with the cost of existing tubes and with the requirements of two potential applications. The estimates, based on scaling the costs of the ETA II now under construction at LLNL, show that the relativitic klystron has the potential to produce rf-power at $<10^{-4}$ \$/rf-watt. Moreover, initial cost sensitivity studies[8] indicate that the LIA-driver characteristics can be optimized to reduce costs at least an additional 20%.

A second example, illustrated in Fig. 6, shows potential costs of using induction linacs to generate high average power submillimeter waves to be used to heat fusion plasmas. Here the estimates are complicated by the fact that LIA voltage and the wavelength of the radiation are intimately linked by basic free-electron laser scaling. Again LIA technology appears capable of delivering power at the requisite scales far beyond the capabilities of present tubes and at strongly competitive prices.

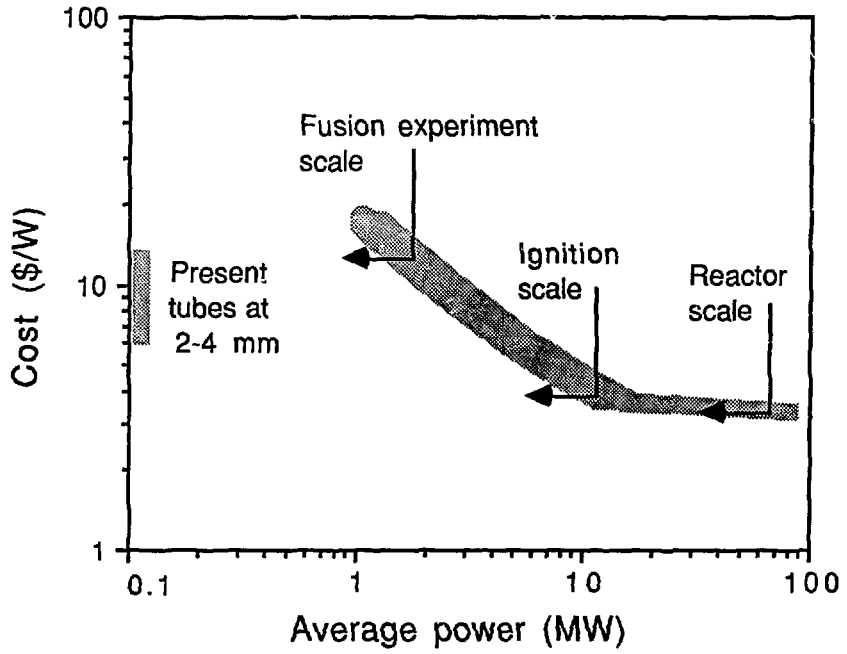

Figure 6. Installed cost of LIA-generated submillimeter wave power.

References

1. R.A. Jameson, "New Linac Technology for SSC and Beyond," in *Proc. 12th International Conf.on High Energy Accelerators, Aug. 11-13, 1983* , FERMILAB, pp. 497 -501.
2. D.B. Hopkins, A.M. Sessler, and J.S. Wurtele, "The Two-Beam Accelerator," *Nuc. Inst. & Meth. for Phys. Res.*, **228**, 15-19 (1984).
3. S.S. Yu and A.M. Sessler, *The Relativistic Klystron Two-Beam Accelerator*, Lawrence Livermore National Laboratory, Livermore, CA, UCRL-96083, (1987), submitted to *Phys. Rev. Lett.*.
4. T. Orzechowski, "High-Efficiency Extraction of Microwave Radiation from a Tapered Wiggler Free Electron Laser, ,*Phys. Rev. Lett.*, **57**, 2172 (1986).
5. K.I. Thomassen, Sci. Ed., *Free Electron Laser Experiments in Alcator C*, Lawrence Livermore National Laboratory, Livermore, CA, LLL-PROP-00202, (1986).
6. W.A. Barletta, *Linear Emittance Damper with Megagauss Fields*, Lawrence Livermore National Laboratory, Livermore, CA, UCRL-96947, (1987).
7. E.P. Lee, *Radiation Damping of Betatron Oscillations*, Lawrence Livermore National Laboratory, Livermore, CA, UCID-19381, (1982).
8. W.A. Barletta, *Cost Optimization of Induction Linac Drives for Linear Colliders*, Lawrence Livermore National Laboratory, Livermore, CA, UCRL-95909, (1986).
9. D. Birx, "The Applications of Magnetic Switches as Pulse Sources for Induction Linacs," *IEEE Transactions in Nuclear Science*, **NS-30**, No. 4, (Aug. 1983).
10. D.L. Birx, G.J. Caporaso, and L.L. Reginato, *Linear Induction Accelerator Parameter Options*, Lawrence Livermore National Laboratory, Livermore, CA, UCID-20786, (1986).
11. D.L. Birx, *A Collection of Thoughts on the Optimization of Magnetically Driven Induction Linacs for the Purpose of Radiation Processing*, Lawrence Livermore National Laboratory, Livermore, CA, UCRL-92828, (1985).
12. G.J. Caporaso, "Control of Beam Dynamics in High Energy Induction Linacs," in *Proc. of LINAC '86 Conference*, (SLAC, July, 1986).
13. G.J. Caporaso, W.A. Barletta, and V.K. Neil, "Transverse Resistive Wall Instability of a Relativistic Electron Beam," *Particle Accelerators*, **11**, pp. 71 - 79, (1980)
14. G.J. Caporaso, "Laser Guiding of Electron Beams in the Advanced Test Accelerator," *Phys. Rev. Lett.*, **57**, no. 13, (1986).

Appendix

Scaling Relations

Variables used in the scaling equations include the total accelerating voltage (V) in MV, the total volt-seconds of core ($W = V T_p$), the gap stress (E_g) in kV/cm, the single pulse energy ($E = VI_{beam}T_p$) in joules, the average power ($P = f E$) in MW, the effective gradient (G) in MV/m, and the inner radius (r_i) in cm. In Eq. (A1) italicized quantities refer to injector voltage, power, pulse energy, etc. Costs are specified in constant FY87 $K.

Injector Subsystem

The scaling equation for the injector is divided into five separate components:

$$C_{inj} = [724\,(W / 0.17)]_{cells} + [475\,(E / 450)]_{mag} + [450\,(P / 2.25)]_{isps} + [165\,(V / 3)^3\,]_{vac} + [60]_{align}\ . \qquad (A1)$$

As each arm of the linear collider is driven by a separate induction linac, this injector cost must be doubled in the estimate of total hardware cost. For most variants of the two-beam accelerator approach this cost is a small fraction of the total.

Beam Transport Subsystems

For solenoidal transport, the cost has three separate components:

$$C_{sol} = [(57+81\,(r_i / 7.5)\,(I / 3000)\,)\,(V / 1.5)\,(I / 3000)\,(r_i / 7.5)\,(0.75 / G)]_{focus} + [42\,(V / 1.5)\,(r_i / 7.5)\,(0.75 / G)]_{steer} + [78]_{match}\ . \qquad (A2)$$

For the alternative laser guiding scheme the scaling equation is

$$C_{laser} = 7.5\ V\ G^{-1}\ , \qquad (A3)$$

which includes laser, gas handling, and matching magnet costs for $f \leq 250$ Hz.

Accelerator Cell Subsystems

The cell block cost is

$$C_{block} = 234\,(V / 1.5)\,(r_o / 20)^2\,(0.75 / G)\,(175 / E_g)\ , \qquad (A4)$$

where r_o is related to r_i by Eq. (9). The ferrite cost is given by

$$C_{ferrite} = 44\,(W / 0.225)\,((r_o + r_i) / 27.5)\ , \qquad (A5)$$

where we have used the relation between the area and volume of the ferrite; Vol = π A (r_o+r_i). The cost of intermediate stores and power supplies scales as

$$C_{isps} = 698\,(P / 3.2) + 5\,(E / 630)\ . \qquad (A6)$$

The scaling for the magnetic pulse compressors is

$$C_{mag} = 241\,(E / 630)\ . \qquad (A7)$$

For power sytems delivering pulses at repetition rates ≈100 Hz the magnetic modulators and intermediate stores can be reengineered to reduce costs by nearly a factor of two. The cost of the strongback alignment structure is

$$C_{strong} = 450\,(V / 12.5)\,(r_o / 20)^2\,(0.75 / G)\,K\ , \qquad (A8)$$

where the constant K depends on the focusing scheme, namely,

$$\begin{aligned} K &= 1.0 \text{ for quadrupoles,} \\ &= 0.6 \text{ for solenoids,} \\ &= 0.5 \text{ for laser guiding.} \end{aligned} \qquad (A9)$$

Ancillary Subsystems

The cost for low and extremely low conductivity water will scale as

$$C_{lcw} = 90\,(P / 13.1) \qquad (A10)$$

for f > 100 Hz. For f < 100 Hz we should use the value of C_{lcw} at f = 100 Hz. The vacuum system is scaled as if it were pumping-speed limited (valid for $r_i \geq 2.5$ cm):

$$C_{vac} = 660\,(V / 12.5)\,(r_i / 7.5)^2\,(0.75 / G)\,K\ , \qquad \text{(A11)}$$

where K is given by Eq. (A9). The cost of electrical fluids is proportional to average beam power;

$$C_{fluid} = 542\,(P / 13.1)\ . \qquad \text{(A12)}$$

The scaling of dump costs is similar to that for reactors, i.e., \$1 per watt of time average beam power into the dump, P_d. For the relativistic klystron we assume that the average beam voltage at the dump (V_d) is 35 MeV; hence,
$P_d = V_d\,T_p\,I_{beam}f$.

The cost of the dump is, therefore,

$$C_{dump} = 1000\,P_d\ . \qquad \text{(A13)}$$

The cost of fixtures is proportional to the length of the induction linac;

$$C_{fixture} = 20\,(V / 12.5)\,(0.75 / G)\ . \qquad \text{(A14)}$$

The cost of the instruments and controls scales as a fixed value plus a percentage of the cost of the hardware to be monitored and controlled;

$$C_{i\&c} = 1500 + 0.04\,(C_{inj} + C_{cell} + C_{focus})\ . \qquad \text{(A15)}$$

Summing the cost equations yields the total hardware cost for the induction linac driver.

Installation and Engineering Support

The installation costs for the base design were estimated on a component by component basis; for estimating purposes the installation costs can be taken as a fixed percentage of the total hardware costs adjusted to the fully loaded labor rate, R, in \$K/man-month.

$$C_{install} = 0.09\,C_{hardware}\,(R / 10)\ . \qquad \text{(A16)}$$

Similarly, a cost for the engineering management and support is estimated as a percentage of the hardware costs, i.e.,

$$C_{engin} = 0.125\,C_{hardware}\ . \qquad \text{(A17)}$$

Supplies and equipment used for engineering and installation increase the total cost by 10%;

$$C_{s\&e} = 0.1\ C_{hardware}\ . \qquad \text{(A18)}$$

Adding these installation costs to the hardware cost yields a total cost which includes ≈10% contingency distributed (unevenly) among the various cost centers.